Physicochem. Probl. Miner. Process., 57(4), 2021, 117-124

http://www.journalssystem.com/ppmp

Physicochemical Problems of Mineral Processing

ISSN 1643-1049
© Wroclaw University of Science and Technology

Received May 07, 2021; reviewed; accepted June 13, 2021

The mechanism of $CaCO_3$ in the gas-based direct reduction of a high-phosphorus oolitic iron ore

Shichao Wu, Zhengyao Li, Tichang Sun, Jue Kou, Chengyan Xu

University of Science and Technology Beijing

Corresponding author: zyli0213@ustb.edu.cn (Zhengyao Li)

Abstract: Gas-based direct reduction and magnetic separation process was applied in treating a high-phosphorus oolitic iron ore, of which phosphorus mainly occured as Fe_3PO_7 and apatite. The mechanism of $CaCO_3$ was investigated using XRD, SEM-EDS, and mineral phase analysis. Results showed that when no $CaCO_3$ was added, most of the iron minerals were reduced to metallic iron, while Fe_3PO_7 was reduced to elemental phosphorus and mixed with the metallic iron particles. When a small amount of $CaCO_3$ was added, $CaCO_3$ preferentially reacted with SiO_2, Al_2O_3 and other components, preventing them from reacting with FeO and resulting in the increase of iron recovery. When the amount of $CaCO_3$ reached 25%, apatite was produced from the reaction of CaO and Fe_3PO_7, which could be later removed by grinding and magnetic separation.

Keywords: high-phosphorus oolitic iron ore, gas-based direct reduction, magnetic separation, Fe_3PO_7, $CaCO_3$

1. Introduction

With the development of the iron and steel industry, high-grade and easy-to-dress iron ores tent to be depleted, and the development of hard-to-dress iron ore has gained increasing attention (Benkli et al., 2018; Gao et al., 2020; Li et al., 2019; Li et al., 2019; Wang et al., 2020). Oolitic iron ore is one of the typical representatives of the refractory iron ore, mainly distributed in France, Germany, the United States, Canada, Russia, Egypt, Saudi Arabia, Pakistan and China (Cha, Kim and Jung 2015; Jonkov et al., 2013; Li et al., 2015; Sun et al. 2013). The oolitic ores have not be well utilized due to the oolitic mineral structure and the high content of phosphorus (Bao, Guo and Guo, 2020; Sun et al., 2017; Tang e al., 2015; Wu et al., 2021). At present, the dilemma in the development of high-phosphorus iron ore lies in the difficulty in achieving high-efficiency removal of phosphorus.

Studies have shown that direct reduction-magnetic separation technique is one of the effective methods for treating high-phosphorus oolitic iron ore (Keith 2018; Zhu et al., 2013). Under optimal conditions, reduced iron was obtained, with iron grade and recovery exceeding 90 wt% and with phosphorus content less than 0.1 wt% (Wu et al., 2015). In this process, additives such as $CaCO_3$, $Ca(OH)_2$, Na_2CO_3 and Na_2SO_4, are often added for upgrading dephosphorization (Keith 2018). Three main dephosphorization mechanisms of the additives are recognized: (1) The additives preferentially react with SiO_2 in the ore to prevent it from promoting the reduction of apatite (Yu et al., 2013; Zhao et al., 2018); (2) Additives destroy the oolitic structure of the ore, promote the reduction of iron minerals and the growth of metallic iron particles, which enables the separation of iron from the phosphorus-containing minerals through grinding and magnetic separation (Li et al., 2012; Li et al., 2013); (3) Additives convert part of phosphorus into easily removable soluble phosphate (Xu et al., 2013; Yang et al., 2010). The application of coal-based direct reduction technology is limited in some areas where coal resources are scarce. Natural gas could be an alternative to coal in this scenario. Compared with coal, it is cleaner to use natural gas for reduction. The use of gas-based reduction is in line with the carbon neutral policy in the global context. However, few studies have been conducted on this topic.

DOI: 10.37190/ppmp/138882

The high-phosphorus oolitic iron ore in this study is located in an area with a rich natural gas reserve but limited coal resources (Yan et al., 2021). Gas-based direct reduction-magnetic separation process was investigated for treating the ore and $CaCO_3$ was used as the additive. Phosphorus in iron ore is mainly in the form of Fe_3PO_7 and apatite (Chen et al., 1999; Huang et al., 2020; Yang et al., 2015). Results showed that the addition of $CaCO_3$ greatly increased the iron recovery rate. With the increase of $CaCO_3$ dosages, the iron recovery rate increased from 57.85 wt% to 92.83 wt%, and the phosphorus content decreased from 0.33 wt% to 0.09 wt% (Yan et al., 2021). It was also found that a large amount of $CaCO_3$, up to 25 wt%, was required for phosphorus reduction even that the phosphorus content of the ore was only 0.72 wt%. To find out why $CaCO_3$ greatly increased the iron recovery rate and why 25 wt% $CaCO_3$ must be added, the mechanism of $CaCO_3$ in the gas-based direct reduction was investigated. The phase transition pattern, the distribution characteristics of phosphorus, the intercalation relationship between iron particles and gangue minerals were studied under different dosages of $CaCO_3$ addition. The study was expected to provide a theoretical basis for gas-based direct reduction application in treating high-phosphorus oolitic iron ores.

2. Experimental

2.1. Materials

The high-phosphorus oolitic iron ore (hereinafter referred to as "raw ore") used in the research was sampled from a mine site. The iron grade of the raw ore is 55.81 wt% and the phosphorus content is 0.72 wt%. SiO_2, Al_2O_3 and CaO are the main impurity components accounting for 5.49 wt%, 4.95 wt% and 2.24 wt%, respectively. The XRD of the raw ore is shown in Fig. 1, the raw ore is mainly composed of hematite, magnetite, siderite, goethite and chlorite. The distribution rates of phosphorus in apatite, Fe_3PO_7 and other minerals are 48.61 wt%, 47.22 wt% and 4.17 wt%, respectively (Huang et al., 2020; Yang et al., 2015). Compared with other high phosphorus oolitic iron ores, the existing state of phosphorus in raw ore is more complicated.

The mixed gas of H_2 and CO was used as the reducing gas. The additive $CaCO_3$ is analytical reagent (AR) grade.

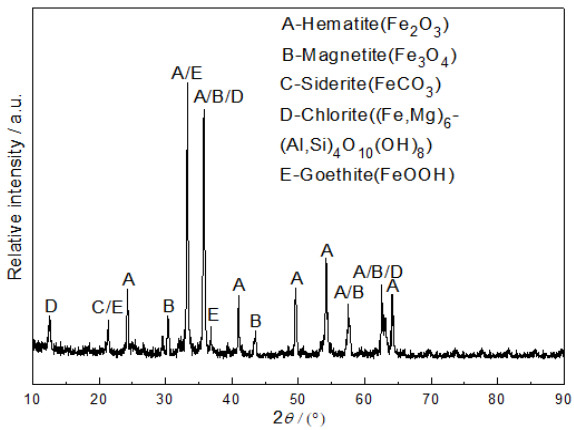

Fig. 1. XRD pattern of raw ore

2.2. Testing method

The test process mainly included pelletizing, gas-based reduction and analysis of roasted products. The testing program is shown in Fig. 2.

(1) Pelletizing. The raw ore with particle size of -1mm, a certain proportion of $CaCO_3$ and 8 wt% water were fully mixed and pressed on roller ball press to form pellets with a diameter of about 18 mm. The green balls were dried in an oven at 105 °C for 4 h until the weight did not change.

(2) Gas-based reduction. The reduction test was carried out in a shaft furnace. When the reduction temperature of the furnace reached 1200 °C, 5 L/min of N_2 was introduced to remove the air in the reaction tube. A hanging basket with two pellets was sent into the reaction tube. N_2 was then stopped, while H_2 and CO were immediately introduced with flow rates of 3.75 L/min and 1.25 L/min,

respectively. When the set reduction time was reached, H_2 and CO valves were closed and N_2 was introduced again with a flow rate of 5 L/min. The hanging basket was taken out and the roasted products were quickly embedded in the graphite powder and cooled to room temperature.

(3) The roasted products were divided into two parts: one part was pulverized to -0.074 mm and analyzed by XRD and phase analysis of phosphorus; the other part was made into optical plate for observing microstructure by SEM-EDS.

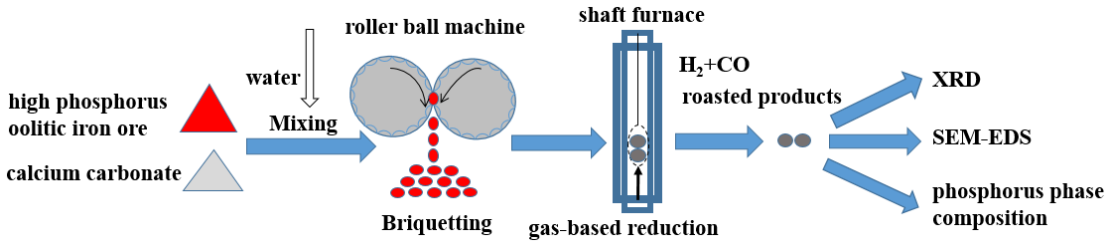

Fig. 2. Experimental procedures for the gas-based reduction process of a high phosphorus oolitic iron ore

3. Results and discussion

3.1. The influence of $CaCO_3$ on the mineral compositions of the roasted products

To find out the effects of $CaCO_3$ on the mineral composition of the roasted products, the phase transition behavior of roasted products was analyzed by X-ray diffraction (XRD). The roasted products were obtained under different $CaCO_3$ dosages at reduction temperature of 1200 °C for 120 min, and under the total flow rate of reducing gas at 5 L/min (H_2 to CO flow ratio 3:1). The results were shown in Fig. 3.

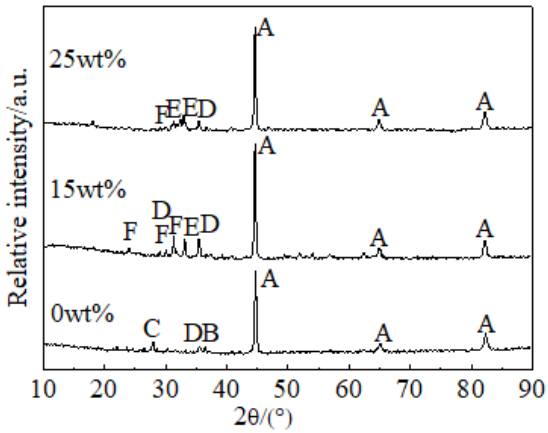

A-Metal iron (Fe); B-Hercynite ($FeAl_2O_4$); C-Anorthite ($CaAl_2Si_2O_8$); D-Pyroxene ($Ca(Fe,Mg)Si_2O_6$); E-Tricalcium silicate (Ca_3SiO_5); F-Gehlenite ($Ca_2Al_2SiO_7$)

Fig. 3. XRD pattern of roasted products under different $CaCO_3$ dosages

It can be seen from Fig. 3 that when $CaCO_3$ was not added, the roasted product was mainly composed of metallic iron and a small amount of pyroxene, hercynite and anorthite, indicating that some iron-bearing minerals, such as hematite and magnetite, were reduced to metallic iron, while a small amount of iron minerals were reduced to FeO. FeO was then transformed to hercynite, pyroxene and anorthite, as Equations (1) and (2).

$$FeO(s) + Al_2O_3(s) = FeAl_2O_4(s) \quad (1)$$

$$CaO(s) + FeO(s) + SiO_2(s) + MgO(s) \rightarrow (Ca(Fe,Mg)Si_2O_6)(s) \quad (2)$$

At $CaCO_3$ dosage of 15 wt%, the roasted product was mainly composed of metallic iron and a small amount of pyroxene, gehlenite and tricalcium silicate. Compared to that when no $CaCO_3$ was added, the diffraction peak intensity of metallic iron and pyroxene was enhanced. The diffraction peaks of hercynite and anorthite disappeared, and gehlenite and tricalcium silicate was newly observed. Results

indicated that CaO preferentially reacted with SiO_2 and generated gehlenite and tricalcium silicate through reaction (3) and (4). Therefore, more FeO was reduced to metallic iron and iron recovery increased. The diffraction peak intensity of pyroxene gradually increased, indicating that reaction (2) was strengthened, and the ferrous iron in pyroxene could not be recovered.

As the $CaCO_3$ dosage increased to 25 wt%, the mineral composition of the roasted product was consistent with that of 15 wt% $CaCO_3$, but with some change in the mineral content. Compared to the results at 15 wt% $CaCO_3$ dosage, the diffraction peak of tricalcium silicate was enhanced, and the intensity of the diffraction peak of pyroxene was weakened, indicating that the reaction (3) was further enhanced, the occurrence of reaction (2) was inhibited, more FeO was reduced to metallic iron and the recovery of iron was further increased.

$$2CaO(s) + 2SiO_2(s) + Al_2O_3(s) = Ca_2Al_2Si_2O_7(s) \quad (3)$$

$$3CaO(s) + SiO_2(s) = Ca_3SiO_5(s) \quad (4)$$

3.2. The influence of $CaCO_3$ on the distribution of phosphorus in the roasted products

The roasted product under different $CaCO_3$ dosage were analyzed for phosphorus phase, and the results as shown in Fig. 4.

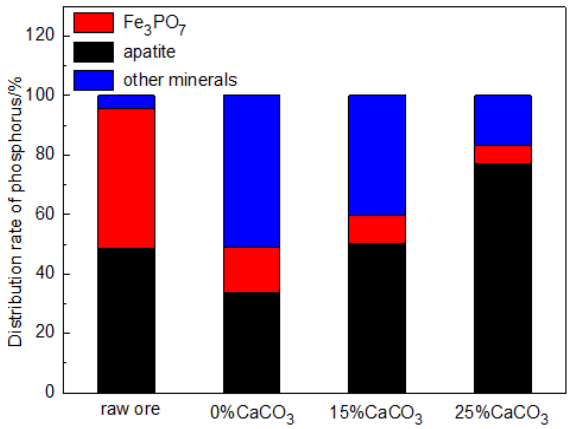

Fig. 4. Phosphorus phase composition of roasted product under different CaCO3 dosages

Results showed that when $CaCO_3$ was not added, the distribution rates of phosphorus in Fe_3PO_7 and apatite in the roasted product were 15.22 wt% and 33.70 wt%, respectively. Compared to that of raw ore, phosphorus as Fe_3PO_7 and apatite decreased, indicating that phosphorus was relocated into other minerals during the reduction. Some of Fe_3PO_7 transformed to phosphoroalumina as equations (5) and (6), while others wewe transformed into elemental phosphorus as equations (7) and (8). The elemental phosphorus reacted with iron and Fe-P alloy was generated as equation (9).

$$2Fe_3PO_7(s) + Al_2O_3(s) + 9CO(g) = 2AlPO_4(s) + 6Fe(s) + 9CO_2(g) \quad (5)$$

$$2Fe_3PO_7(s) + Al_2O_3(s) + 9H_2(g) = 2AlPO_4(s) + 6Fe(s) + 9H_2O(g) \quad (6)$$

$$2Fe_3PO_7(s) + 14CO(g) = P_2 + 6Fe(s) + 14CO_2(g) \quad (7)$$

$$2Fe_3PO_7(s) + 14H_2(g) = P_2 + 6Fe(s) + 14H_2O(g) \quad (8)$$

$$6Fe(s) + P_2(g) = 2Fe_3P(s) \quad (9)$$

With the increase of $CaCO_3$ dosages, the phosphorus in the apatite gradually increased, indicating that the phosphorus was enriched in apatite in the roasted product. At $CaCO_3$ dosage of 25 wt%, the phosphorus distributed in apatite increased to 76.92 wt%, and the phosphorus distribution rate in Fe_3PO_7 dropped to 6.41 wt%, which indicated that CaO reacted with Fe_3PO_7 and generated apatite, as equations (10) and (11). In addition, CaO preferentially reacted with SiO_2 in the ore to prevent SiO_2 participating the reduction of apatite which promoted the iron recovery.

$$2Fe_3PO_7(s) + 3CaO(s) + 9CO(g) = Ca_3(PO_4)_2(s) + 6Fe(s) + 9CO_2(g) \quad (10)$$

$$2Fe_3PO_7(s) + 3CaO(s) + 9H_2(g) = Ca_3(PO_4)_2(s) + 6Fe(s) + 9H_2O(g) \quad (11)$$

For the investigated ore, the phosphorus content in the form of Fe_3PO_7 is 0.34%. If $CaCO_3$ only participated in reaction 8) and reaction (9), only a small amount of $CaCO_3$ would be needed in its reaction with Fe_3PO_7 and producing apatite, however, test results showed that the minimum 25% $CaCO_3$ should be in fact required in the phosphorus reduction. This is because some CaO, decomposed from $CaCO_3$, preferentially reacted with SiO_2, Al_2O_3 and other components in the ore and formed gehlenite and tricalcium silicate, therefore more $CaCO_3$ should be added in order to satisfy the need of the phosphorus reduction. Only when the amount of $CaCO_3$ reached 25%, the decomposed CaO would be sufficient to completely reduce the Fe_3PO_7 into apatite.

3.3. The influence of $CaCO_3$ on the microstructure of the roasted products

To further clarify the dephosphorization mechanism of $CaCO_3$ in the gas-based reduction, SEM-EDS analysis was carried out on roasted products under different $CaCO_3$ dosages. The influence of $CaCO_3$ dosages on the iron particle size, the relationship between iron particles and other minerals, the distribution of phosphorus and the relationship between phosphorus and metal iron particles were investigated. The results were shown in Fig. 5.

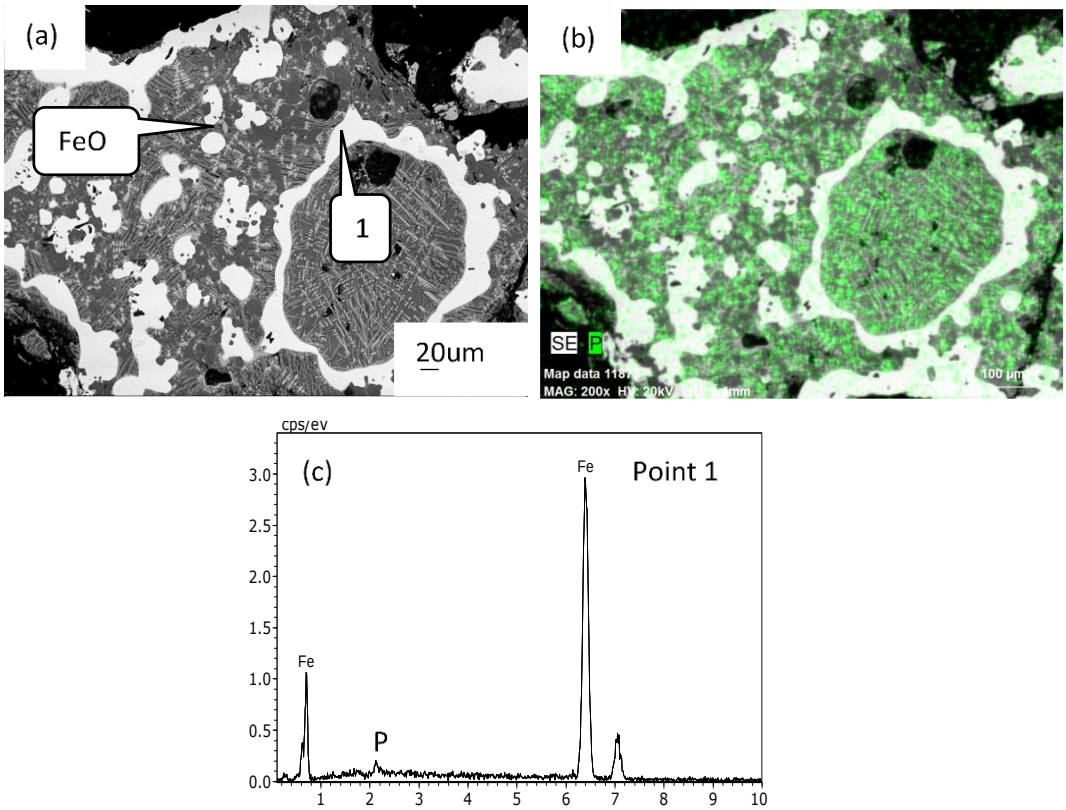

Fig. 5. SEM-EDS images of roasted product without $CaCO_3$: (a) SEM image; (b) the surface scan of phosphorus element in image (a); (c)EDS spectrum of Point 1

Fig. 5 showed the SEM-EDS image of the roasted product without the addition of $CaCO_3$. It can be seen from Fig. 5(a) that the oolitic structure of the raw ore was completely destroyed after roasting; most of generated metal iron (white particles) had a particle size of more than 30 µm; the iron particles were mainly short-chained and rod-like and had a clear boundary with the gangue minerals. Magnetic separation results showed that iron product was obtained with grade of over 90 wt%. However, the recovery rate of iron was low, as the reducing gas was difficult to diffuse and the fusoid outside the metal iron shell could not be reduced. Fig. 5(b) showed that most of the phosphorus in the roasted product was evenly distributed in the gangue, while a small amount was finely scattered in the iron particles. The observations were consistent with Fig. 4 when $CaCO_3$ was not added. The energy spectrum of point 1 showed that the phosphorus was contained in metallic iron particles and formed iron-phosphorus alloy, indicating that the reaction (7)-(9) occurred. It should be noted that phosphorus

in form of alloy cannot be separated by magnetic separation. Therefore, the phosphorus content in the iron product was relatively high.

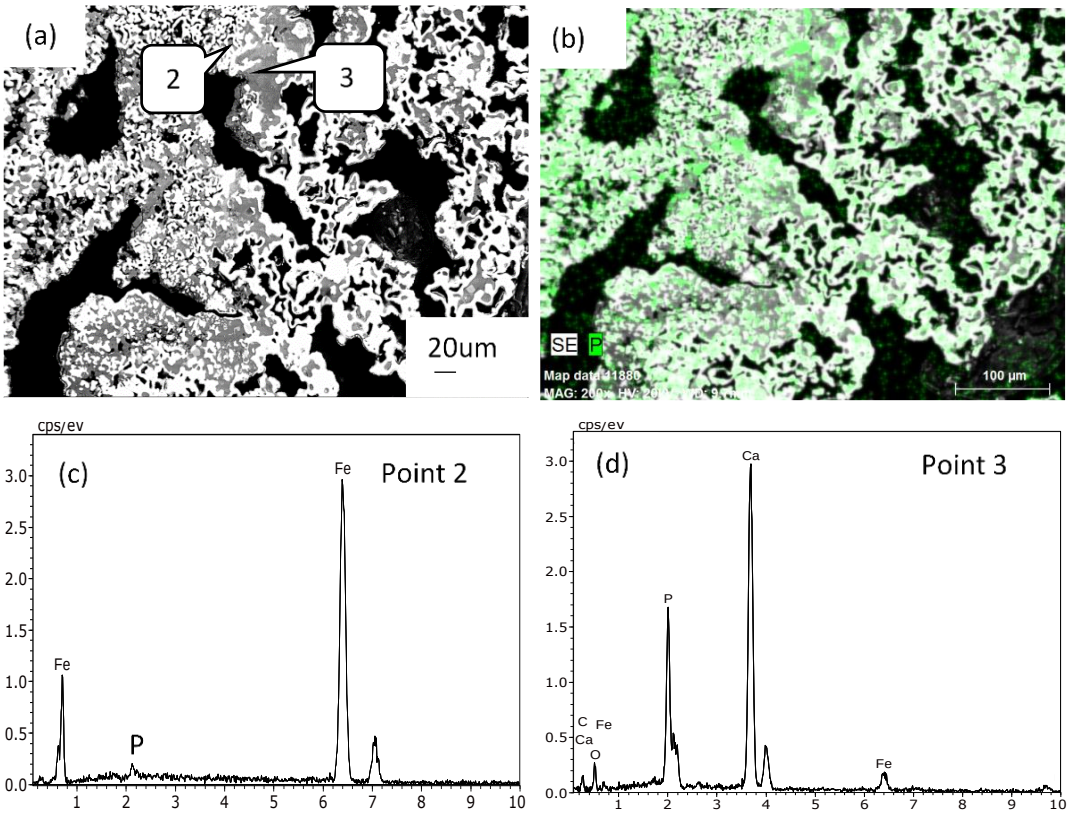

Fig. 6. SEM-EDS images of roasted product with 15% CaCO3: (a) SEM image; (b) the surface scan of phosphorus element in image (a); (c)EDS spectrum of Point 2; (d) EDS spectrum of Point 3

Fig. 6 showed the SEM-EDS diagram of roasted products with 15 wt% $CaCO_3$. It can be seen from Fig. 6(a) that, compared to that without $CaCO_3$ addition, the microstructure of the roasted product changed significantly. The oolitic structure was destroyed completely while the melting was lightened. Some gangue minerals were mixed with the metal iron particles, which decreased the grade of the iron product. The iron particles became smaller and the number of the particles increased significantly, indicating the reduction of iron-bearing minerals into metallic iron and the increased iron recovery rate.

Fig. 6(b) showed that phosphorus was mainly distributed in the form of tiny granular apatite around the iron particles, while a trace amount of phosphorus was distributed in the metallic iron particles. The energy spectra of points 2 and 3 showed that phosphorus was contained in the metallic iron particles near the apatite. This is because that $CaCO_3$ preferentially reacted with the gangue minerals and only part of Fe_3PO_7 was reduced into apatite, resulting in that a small amount of Fe_3PO_7 was still reduced to elemental phosphorus and mixed into the iron particles.

Fig. 7 showed the SEM-EDS análisis results of the roasted product at $CaCO_3$ dosage of 25 wt%. Fig. 7(a) showed that the oolitic structure in the raw ore was also destroyed. Compared to that at 15 wt% dosage, the iron particles were separated and the size of the iron particles increased, which facilitated the liberation of the iron particles during subsequent grinding. Therefore, the iron grade and iron recovery of the reduced iron obtained by magnetic separation were improved. It can be seen from Fig. 7(b) that phosphorus was mainly distributed in fine apatite which clearly margined from iron particles. This is the same as Fig. 2 where 76.92 wt% of phosphorus occured in the form of apatite. This further proved that $CaCO_3$ reacted with Fe_3PO_7 and formed aggregated apatite. The energy spectrum at point 3 showed that the metallic iron particles did not contain phosphorus, indicating that sufficient $CaCO_3$ and Fe_3PO_7 fully reacted into apatite, so that the iron particles and apatite would be effectively separated during the subsequent grinding and magnetic separation. In summary, we find that the dephosphorization mechanism obtained in this paper is different from previous studies.

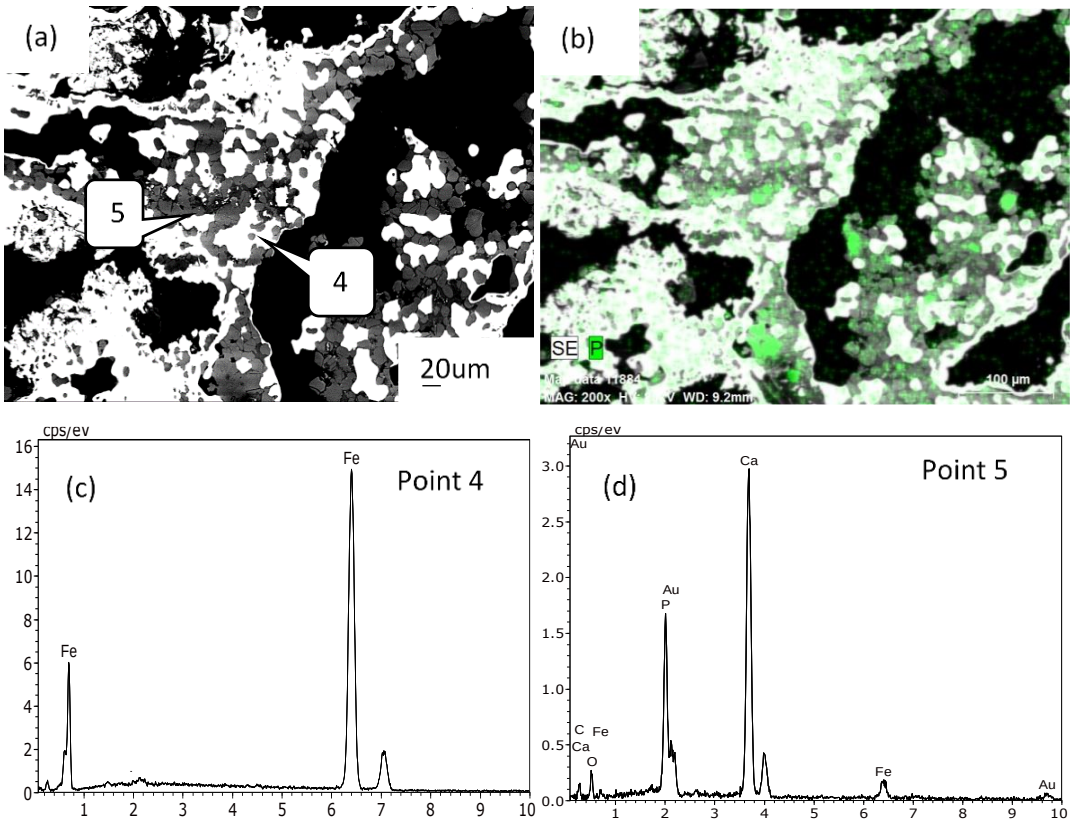

Fig. 7. SEM-EDS images of roasted product with 25 wt% CaCO3 (a) SEM image; (b) the surface scan of phosphorus element in image (a); (c)EDS spectrum of Point 4; (d) EDS spectrum of Point 5

4. Conclusions

The conclusions of this study are as follows:

(1) When no $CaCO_3$ was added, a small amount of hercynite and pyroxene was formed; melting was prone to occur during the roasting where the reducing gas was difficult to diffuse and wrapped by the metal iron shell, resulting in the formation of holes outside the shell. Iron-phosphorus alloy was formed from a part of Fe_3PO_7.

(2) When $CaCO_3$ was added, $CaCO_3$ preferentially reacted with SiO_2, Al_2O_3 and other components and formed leucoside and tricalcium silicate, which prevented SiO_2 from reacting with FeO and promoted the recovery of iron.

(3) At $CaCO_3$ dosage of 25 wt%, the decomposed CaO was sufficient to react with Fe_3PO_7. Monolith apatite was formed and had obvious boundary with iron particles. The iron particles could be effectively separated from apatite by grinding and magnetic separation, and therefore phosphorus was effectively removed from the iron product.

Acknowledgments

This work was financially supported by the National Nature Science Foundation of China (Grant No. 51874017).

References

BAO, Q.P., GUO, L., GUO, Z.C., 2020. *A novel direct reduction-flash smelting separation process of treating high phosphorous iron ore fines.* Powder Technol. 377, 149-162.

BENKLI, Y.E., BOYRAZLI, MUSTAFA, SENOZ, G. M. L., CIZMECIOGLU, Z., 2018. *Investigation of reduction of magnetite based carbon composite pellets under semi-fusion conditions.* Physicochem. Probl. Mineral Pro. 54(3), 621-628.

CHA, J.W., KIM, D.Y., JUNG, S.M., 2015. *Distribution behavior of phosphorus and metallization of iron oxide in carbothermic reduction of high-phosphorus iron ore.* Metall. Mater. Trans. B. 46(5), 2165-2179.

CHENG, C.Y., MISRA, V.N., CLOUGH, J., MUNI R., 1999. *Dephosphorisation of Western Australian iron ore by hydrometallurgical process.* Miner. Eng. 12(9), 1083-1092.

GAO, P., AN, Y.X., LI, G.F., HAN, Y.X., 2020. *Effect of particle size on reduction kinetics of hematite ore in suspension roaster Physicochem.* Physicochem. Probl. Mineral Pro. 56(3), 449-459.

HUANG, W.S., YAN, L., WU, S.C., SUN T.C., 2020. *Study on the process mineralogy of a high phosphorus ooliticiron ore in abroad.* Met. Mine. 9, 137-141.

IONKOV, K., GAYDARDZHIEV, S., ARAUJO, A. C., BASTIN, D., LACOSTE, M., 2013. *Amenability for processing of oolitic iron ore concentrate for phosphorus removal.* Miner. Eng. 46-47, 119-127.

KEITH, Q., 2018. *A review on the characterisation and processing of oolitic iron ores.* Miner. Eng. 126, 89-102.

LI, G.H., RAO, M.J., OUYANG, C.Z., ZHANG, S.H., PENG Z.W., JIANG, T., 2015. *Distribution characteristics of phosphorus in the metallic iron during solid-state reductive roasting of oolitic hematite ore.* ISIJ Int. 55(11), 2304-2309.

LI, G.H., ZHANG, S.H., RAO, M.J., ZHANG, Y.B., JIANG, T., 2013. *Effects of sodium salts on reduction roasting and Fe-P separation of high-phosphorus oolitic hematite ore.* Int. J. Miner. Process. 124, 26-34.

LI, W.B., HAN, Y.X., LIU, X., SHAN, Y, LI, Y.J., 2019. *Effect of fluidized magnetizing roasting on iron recovery and transformation of weakly magnetic iron mineral phase in iron tailings*. Physicochem. Probl. Mineral Pro. 55(4), 906-916.

LI, X.H., KOU, J., SUN, T.C., WU, S.C., ZHAO, Y.Q., 2019. *Effects of Temperature on Fe and Ti in Carbothermic Reduction of Vanadium Titanomagnetite with adding MgO.* Physicochem. Probl. Mineral Pro. 55(4), 917-927.

LI, Y.L., SUN, T.C., XU, C.Y., LIU, Z.H., 2012. *New dephosphorizing agent for phosphorus removal from high-phosphorus oolitic hematite ore in direct reduction roasting*. J Cent. South. Univ. (Sci Technol). 43(3), 827-834.

SUN, Y.S., GAO, P., HAN, Y.X., REN, D.Z., 2013. *Reaction behavior of iron minerals and metallic iron particles growth in coal-based Reduction of an oolitic iron ore.* Ind. Eng. Chem. Res. 52(6), 2323-2329.

SUN, Y.S., HAN, Y.X., LI, Y.F., LI, Y.J., 2017. *Formation and characterization of metallic iron grains in coal-based reduction of oolitic iron ore.* Int. J. Miner. Metall. Mater. 24(2), 123-129.

TANG, H.Q., QI, T.F., QIN, Y.Q., 2015. *Production of low-phosphorus molten iron from high- phosphorus oolitic hematite using biomass char.* JOM. 67(9), 1956-1965.

TANG, Z.D., GAO, P., SUN, Y.S., HAN, Y.X., LI, E.L., CHEN, J., ZHANG, Y.H., 2020. *Studies on the fluidization performance of a novel fluidized bed reactor for iron ore suspension roasting.* Powder Technol. 360, 649-657.

WANG, X.P., SUN, T.C., WU, S.C., HU, T.Y., RONG, L.K., 2020. *Effects and mechanism of Bayer red mud on co-reduction with a saprolitic laterite ore to prepare ferronickel Physicochem.* Physicochem. Probl. Mineral Pro.. 56(4), 2020, 641-652.

WU, S.C., SUN, T.C., LI, Z.Y., XU, C.Y., LI, X.H., 2021. *Research progress of direct reduction-magnetic separation of high phosphorus iron ore.* Met. Mine. 2, 58-64.

XU, Y., SUN, T.C., LIU, Z.G., LIU, Z.H., 2013. *Phosphorus occurrence state and phosphorus removal research of a high phosphorous oolitic hematite by direct reduction roasting method.* J. North. Univ (Nat. Sci.). 34(11), 1651-1655.

YAN, L., HUANG, W.S., WU, S.C., SUN, T.C., 2021. *High-phosphorus oolitic iron ore processed with gas-based direct reduction and magnetic separation for iron increasing and phosphorus reduction*. Min Metall Eng. 41(1), 72-75.

YANG, D.W., SUN, T.C., YANG, H.F., XU, C.Y., QI, C.Y., LI, Z.X., 2010. *Dephosphorization mechanism in a roasting process for directreduction of high-phosphorus oolitic hematite in west Hubei Province*. Chin. J. Univ. Sci. Technol. Bei. 32(8), 968-974.

YANG, M., ZHU, Q.S., FAN, C.L., XIE, Z.H., LI, H.Z., 2015. *Roasting-induced phase change and its influence on phosphorus removal through acid leaching for high-phosphorus iron ore*. Int. J. Miner. Metall. Mater. 22(4), 346-352.

YU, W., SUN, T.C., KOU, J., WEI, Y.X., XU, C.Y., LIU, Z.Z., 2013. *The function of $Ca(OH)_2$ and Na_2CO_3 as additive on the reduction of high-phosphorus oolitic hematite-coal mixed pellets.* ISIJ Int. 53(3), 427-433.

ZHAO, Y.Q., SUN, T.C., ZHAO H.Y., LI, X.H., WANG, X.P., 2018. *Effects of $CaCO_3$ as additive on coal-based reduction of high-phosphorus oolitic hematite ore.* ISIJ Int. 58(10), 1768-1774.

ZHU, D.Q., CHUN, T.J., PAN, J., LU, L.M., HE, Z., 2013. *Upgrading and dephosphorization of Western Australian iron ore using reduction roasting by adding sodium carbonate*. Int. J. Miner. Metall. Mater. 20(6), 505-513.